Published by :
http://www.ijert.org

International Journal of Engineering Research & Technology (IJERT)
ISSN: 2278-0181
Vol. 5 Issue 01, January-2016

Heat Transient in the Circular Finned Cylindrical pipe with the Application of an Off-feed Axis Solar Concentrating Collector

Appu Kumar Singh
Department of Mechanical Engineering,
Bhilai Institute of Technology Raipur
Raipur, India

Akansha Singh
School of Mechanical Engineering
Kalinga Institute of Industrial Technology
Bhubaneswar, Odisha, India

***Abstract*—The selected contemporary project will address how the unsteady state in convective and radiative heat transfer infers in the circular finned cylindrical pipes under solar load. Both analytical and numerical solutions of the governing finite element non-linear problems are presented. Transient temperature profile distribution is determined using Stefan – Boltzmann's theory and for the thermal stress due to temperature gradient with the material mix, the von misses yield criterion in combination with an iterative scheme is used. Moreover, a thick cylindrical pressure vessel and parabolic collector are also designed and presented here. Governing equations related to the analyzed data are applied and designed a prototype model. The simulation presented provides the satisfactory prediction of performance as compared to the designed data. Shortcomings of the methodology are highlighted and an alternative approach to solving particulars suggested.**

Keywords—Prototype Model, Transient, Governing Equations

I. INTRODUCTION

There are certain ways to implement function application in a non-linear differential equation, when the function is unknown; the numerical model or trial or error model is provoked. To illustrate the difference, consider the non-homogenous first order differential equation, which is applied to a body. And from the equation, transient convection and transient radiation are to be evaluated:

$$- [h (T - T_\infty) + \varepsilon \sigma (T^4 - T^4_{sur})] A_s = \rho V c \frac{dT}{d\Gamma} \qquad (1)$$

Here temperature, T = f (Γ), is an unknown function; global transient thermal flow analysis aside, the compiler does not know what function T is bound to. How should the compiler deal with the call f (Γ) in the thermal bounded body? It can't be blithely applied, by calculating integrating factor:

$$\int M\,dx + \int (terms\ of N\ not\ containing\ x)\,dy = c \qquad (2)$$

In practice, a numerical model is prepared and a trial or error is implied or either the numerical integration by Simpson's one-third rule or Runge - Kutta's method with an iterative scheme; in which finding the increment k of f(Γ), corresponding to an increment h of f(T).

Which of the two is best in practice? The trouble is that the evaluation model has a pervasive effect on the implementation, so it is too much working steps to implement both and pick the best. In alter practice, implementers choose one of the approaches based on a qualitative assessment, i.e., boundary conditions and assumptions, of the trade-offs. In this paper, we put the choices on a firmer basis:

- We explain precisely what the numerical models are, in a Finite Element method (Section - 5).
- The choice of evaluation model affects many other design aspects in subtle but pervasive ways. We identify and discuss these effects in sections 5 and 6, and contrast them in section 7. Articulating these details is one of our main contributions.
- We prove that the material choice will not affect the stresses; it will only affect the displacements and strains, in the thick pressure vessel (section – 5.A).
- We found that the maximum hoop stresses using the thin-wall and thick-wall approximations yield corresponds to a 16% difference which tells us that the thin wall theory might not be adequate for illustrated geometry (section – 7). The thin - wall theory actually gives good results when b/a ratio is less than 1.10.
- Also proved that the axial stresses are constant for both theories, i.e., the thin-wall and thick-wall; since they do not depend on radius (section – 5.A).
- We also observed that the high heat flux density occurs at the exact point where the fins begin. It's difficult for the gamma energy to enter the large surface area of the rib, showing casting boundary effects (section – 5.B).

In terms of its impact on time frame and heat flow system complexity, evaluation seems decisively superior, principally because the design is safe, according to the von Mises theory or maximum distortion energy theory of failure yield criterion.

A. Background

To set the scene for this paper, we begin with a brief overview of the failure theory of yield criterion. Commonly, for ductile materials such as structural steel (grade – St-32), there are two important yield criteria. They are von Mises yield criterion – also called distortion energy criterion and Tresca criterion also called Maximum shear stress theory.

International Journal of Engineering Research & Technology (IJERT)
ISSN: 2278-0181
Vol. 5 Issue 01, January-2016

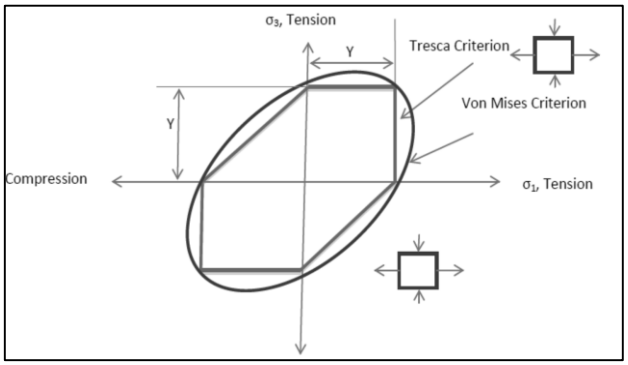

Fig. 1. Showing the yield criteria for the von Mises and the Tresca criterion

However, the von Mises yield criterion is found to be suitable for most of the ductile materials because the von Mises criterion is able to predict the yielding independent of the sign of the stresses because this criterion has square terms of the shear stresses [10].

Therefore, according to the von Mises or maximum distortion energy theory, if the maximum distortion energy exceeds the distortion energy at the tensile yield point failure occurs [10].

II. DESIGN

A. *Design of Parabolic Collector*

An asymmetrical segment of a paraboloid is utilized as a reflector, here the focus and the feed section are located to one side of the dish or positioned as an offset to the axis.

This design increases the area for radiation reception, so more energy can be accumulated at the focus after reflection [6].

An offset-feed dish has higher efficiency than a conventional dish of the same aperture. Parabolic antennas are based on the geometrical property of the paraboloid that all the paths are of the same length. So, a spherical wave front emitted by a feed antenna at the dish's focus will be reflected into an outgoing plane wave travelling parallel to the dish's axis.

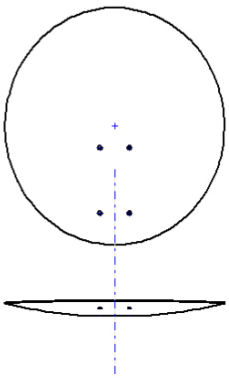

Fig. 2.1. Geometric view of the parabolic collector

The height, width and the maximum depth of the paraboloid are measured taking reference from the edge across the dish from top to bottom; used to calculate the focal length of the dish. The length of material is 600 mm and height of the aluminum material is 555 mm.

Following is the Legon's design equation to calculate the focal length of an offset dish antenna.

$$\text{Focal length} = (\text{width})^3 / (16 \times \text{depth} \times \text{height}) \quad (3)$$

The focal point is made at the distance of 400 mm. An ordinary solar reflective film has 78% heat reflective property.

B. *Design of Thick Pressure Vessel*

Fig. 2.2. SolidWorks® 2015 Thick Pressure vessel Design Model

Above design is the pressurized thick-walled hydraulic cylinder. The following figure 2.2 shows a section through the mid-plane.

Stress directions in cylindrical coordinates are represented in figure 1. σ_h is in the circumferential direction (out of the plane here); r_i= inner radius = 15.56 mm; 285 mm long and r are the radial position.

Here, we will be describing in to find the σ_h (hoop stress), σ_a (axial stress) and σ_r (radial stress) at the mid-length of the cylinders, to neglect the local effects of the end caps.

For this problem, the material choice will not affect the stresses; it will only affect the displacements and strains. Relative straightforward axisymmetric FEA has been applied and hence resolved a solution.

TABLE I. STRUCTURAL STEEL MATERIAL DATA

Density	7.85e-006 kg mm^-3
Coefficient of Thermal Expansion	1.2e-005 C^-1
Specific Heat	4.34e+005 mJ kg^-1 C^-1
Thermal Conductivity	6.05e-002 W mm^-1 C^-1
Resistivity	1.7e-004 ohm mm
Yield Strength M Pa	250
Tensile Ultimate Strength M Pa	460

Designing the thick pressure vessel by applying von Mises failure theory of yield criterion [10].

$$E_d = \frac{1+\nu}{6E}\{(\sigma_1-\sigma_2)^2+(\sigma_2-\sigma_3)^2+(\sigma_3-\sigma_1)^2\} \quad (4)$$

At the uniaxial tensile yield point $\sigma_2 = \sigma_3 = 0$, $\sigma_1 = \sigma_y$. Also, considering $\sigma_h = \sigma_1$, $\sigma_a = \sigma_3$ and $\sigma_r = \sigma_2$. Therefore,

$$\text{Inner surface Hoops stress, } \sigma_h = p_i \frac{(r_0^2+r_i^2)}{(r_0^2-r_i^2)} \quad (5)$$

International Journal of Engineering Research & Technology (IJERT)
ISSN: 2278-0181
Vol. 5 Issue 01, January-2016

Outer surface Hoops stress, σ_h = $p_i \frac{p_i r_i^2}{r^2} \frac{(r_0^2+r^2)}{(r_0^2-r_i^2)}$ (6)

$$\sigma_r = - p_i \quad (7)$$

$$\sigma_a = \frac{p_i r_i^2}{(r_0^2-r_i^2)} \quad (8)$$

Axial Stress, σ_a is same for throughout any region of the thick cylinder pressure vessel. Henceforth, solving the failure criterion therefore reduces to,

$$\frac{p_i}{\sigma_y} = \frac{1}{\sqrt{3}} \frac{(r_0^2 - r_i^2)}{r_0^2} \quad (9)$$

$$\text{Thickness, } t = r_i \left(\frac{1}{\sqrt{\left(1-\sqrt{3}\left(\frac{p_i}{\sigma_y}\right)\right)}} - 1 \right) \quad (10)$$

The allowable safe stress (σ_s) is equal to the ultimate stress divided by the factor of safety (n). Taking n = 2.8,

$$\sigma_s = \frac{\sigma_u}{n} = 164.28 \text{ Mpa} \quad (11)$$

Substituting $\sigma_s = \sigma_y$ and the value of r_0, r_i in the above equations and solving,

TABLE II. THICK PRESSURE VESSEL ANALYTICAL RESULTS

		Parameters
Hoop Stress (M pa)	*Inner Surface*	181.06
	Outer Surface	172.43
Axial Stress (M pa)	*(Constant)*	86.21
Radial Stress (M pa)	*Inner Surface*	-8.628
	Outer Surface	0
Internal Pressure (M pa)		8.628
Thickness (mm)		0.76

III. EXPERIMENTAL SETUP

The experimental arrangement comprises an off-feed axis parabolic dish concentrating collector which is made up of a dish concentrator and a thermal reflector.

A thick cylinder pressure vessel located at the focus of the dish. A circular finned cylindrical heat exchanger pipe is installed at the exit of the pressure vessel. For water supply, a pipe is installed to the set-up.

Fig. 3. SolidWorks®2015 rendering of proposed model

The experimental set-up tracks the sun and focuses solar energy into a cavity absorber through parabolic collector. Solar energy is absorbed and transferred to the pressure vessel, where the water heats up and being converted into steam. The steam is then entered into the circular finned cylindrical pipe heat exchanger.

IV. CALCULATION

The World Radiation Centre (WRC) has adopted a value of the solar constant as, I_{sc} = 1367 W/m^2 (1.940 Cal/cm^{2}min., 432 Btu/ft^2 or 4.921 MJ/m^{2}hr.) [2]. It has been accepted universally as a standard value of the solar constant.

According to the location and time, following parameters are observed:

Location: Bishrampur, Chhattisgarh, India

Longitude: 23.1897° N

Latitude: 83.0047° E

IST: 06:38 to 17:26 hr. (From sunrise to sunset)

Ambient temperature: 24°C (daily basis temperature for the date)

No. of days (n) =3 days: 3rd of January, 2016 (from 1st of January, 2016)

Humidity: 23 %

Wind speed: 4 km/h

The extra-terrestrial radiation deviates from the solar constant value, hence given by [2]:

$$I_{ext} = I_{sc}[1.0+0.033 \cos\left(\frac{360n}{365}\right)] \quad (12)$$

Beam radiation received on earth per sq. m on a plane surface normal to the direction of radiation, may be estimated as [2]:

$$I_N = I_{ext}\, e^{[-T_R/(0.9+9.4\sin\alpha]}} \quad (13)$$

International Journal of Engineering Research & Technology (IJERT)
ISSN: 2278-0181
Vol. 5 Issue 01, January-2016

Where, T_R (turbidity factor) for mountain =1.8, α (inclination angle) =45˚

Normal beam radiation I_b, and diffuse radiation I_d, on the horizontal surface are recorded from the following expressions [2]:

$$I_b = I_N \cos\theta_z \quad (14)$$

Declination,

$$\delta = 23.45 \times \sin\left[\frac{360}{365}(284 + n)\right] \quad (15)$$

The equation of time E, can be found out from the following expressions [1]:

$$E = 9.87 \sin 2B - 7.53 \cos B - 1.5 \sin B \quad (16)$$

Where B= (360/364) (n-81) = -77.14

The standard time is converted into solar time as follows [1]:

$$\text{Solar time} = \text{Standard time} \pm 4(L_{st} - L_{loc}) + E \quad (17)$$

Zenith angle θ_z, for the horizontal surface can be found out from the following expressions [1]:

$$\cos\theta_z = \cos\phi \cos\delta \cos\omega + \sin\delta \sin\phi \quad (18)$$

$$I_d = (1/3)(I_{ext} - I_N)\cos\theta_z \quad (19)$$

Total radiation on the Earth's surface [2]:

$$I_T = I_b R_b + I_d R_d + R_r (I_b + I_d) \quad (20)$$

R_b, ratio of flux beam radiation on an inclined surface to a horizontal surface,

For a vertical surface facing due south [1]:

$$\cos\theta_i = -\sin\delta \cos\phi + \cos\delta \cos\omega \sin\phi \quad (21)$$

$$R_b = \frac{\cos\theta_i}{\cos\theta_z} \quad (22)$$

R_d, ratio of flux of the diffused radiation falling on inclined surface to a horizontal surface,

$$R_d = \frac{1+\cos\beta}{2} \quad (23)$$

R_r, the reflected component comes mainly from the ground and the surrounding objects,

$$R_r = \rho\left(\frac{1-\cos\beta}{2}\right) \quad (24)$$

Where ρ= ground reflection coefficient

$I_T = 773.88 \times 0.178 + 69.48 \times 0.5 + 0.1(773.88 + 69.48)$

$= 256.825 \text{ W/m}^2$

Now, the concentration ratio can be given as [3]:

$$C \text{ (Conc. Ratio)} = \frac{\text{aperture area of concentrator}}{\text{area of absorber}} = 814.87 \quad (25)$$

From Stefan- Boltzmann law, to predict the performance of a solar collector it is necessary to evaluate the radiation exchange between the non- black bodies [4]:

$$Q_{net} = f_{12} F_{12} \sigma_b A_1 (T_1^4 - T_2^4) \quad (26)$$

Where $f_{12} = \varepsilon_1$ represents the equivalent emissivity between the small body and enclosure or interchange factor= 0.78; F_{12}= geometric factor= 1,

Fig. 4. Image depicting temperature T_1, 380° C

$$Q_{net} = 1 \times 0.78 \times 5.67 \times 10^{-8} \times 0.256(380^4 - 24^4) = 1.97 \text{ KW}$$

V. SIMULATION

A. *Static Structural Analysis of Thick Cylinder Pressure Vessel*

For Axis-symmetric FEA study, an element size of the geometry model of outer diameter 32.64mm, thickness of 0.76mm and depth 10mm has been modelled.

Applied Material is structural steel. Generating optimal coarse mesh using mapped face meshing of element size of 0.01 mm.

Symmetry boundary condition at the top edge implies zero displacement in the axial direction. The top edge represents a plane of symmetry since it is located at the mid-length of the cylinder and we are modeling only half the length. Imposing the symmetry boundary condition using a "Frictionless support".

International Journal of Engineering Research & Technology (IJERT)
ISSN: 2278-0181
Vol. 5 Issue 01, January-2016

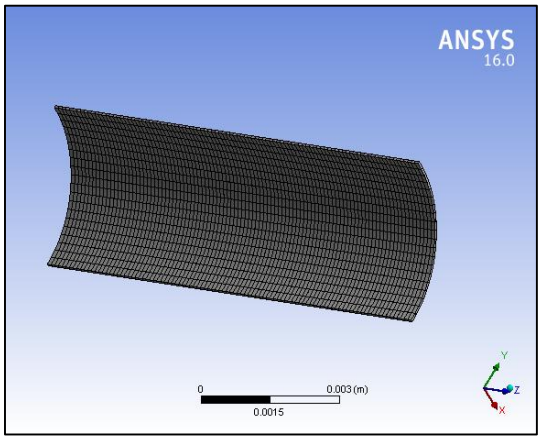

Fig. 5.1. Ansys®16.0 Element Model being meshed

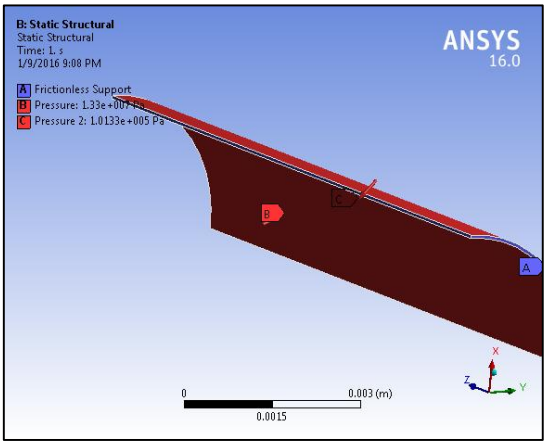

Fig. 5.2. Ansys®16.0 Element Model being meshed and Boundary conditions applied

In an axisymmetric model, no displacement constraints are necessary in the radial direction to prevent rigid body motion in that direction. This is because the radial displacement represents an expansion / contraction of the structure which is resisted structurally.

The following figure 5.2 shows the specification of the physics of the problem: axisymmetric analysis, material properties (Young's modulus and Poisson ratio by default) and boundary conditions. These settings get fed into the element formulation when obtaining the numerical solution.

To obtain the numerical solution, formation of the local stiffness matrix for each element occurs. Thereafter, assembling into the global stiffness matrix and inverted it to get the nodal displacements. This is the bulk of the computation that FEA performs.

All the results that we will look at the next such as the deformed shape and the stresses are derived from these nodal displacements.

Applying a load onto two surfaces, pressure on the inside surface 8.628 M Pa and atmospheric pressure on the outer surface.

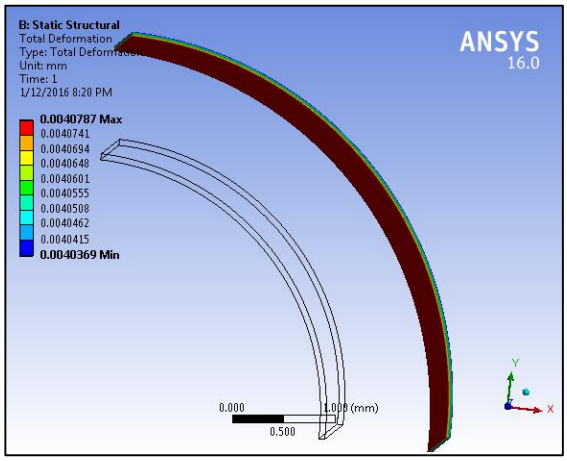

Fig. 5.3. Ansys®16.0 Showing Element Model deformation (Scale 2.0)

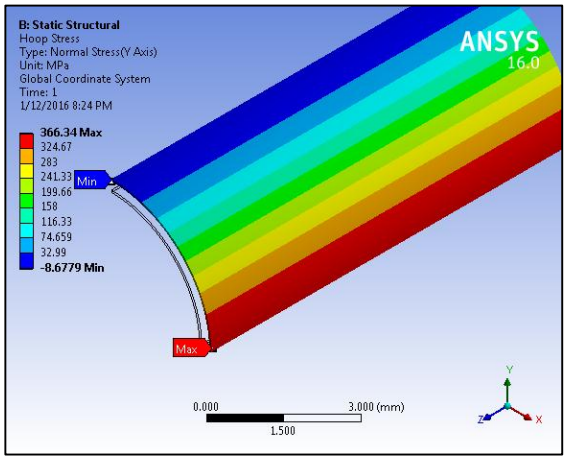

Fig. 5.4. Ansys®16.0 Showing Element Model deformation and Hoops stress distribution

Pascal's total deformation (Scale 2.0) is very small of current law to be applied and very small stresses on progressing to the application one Pascal.

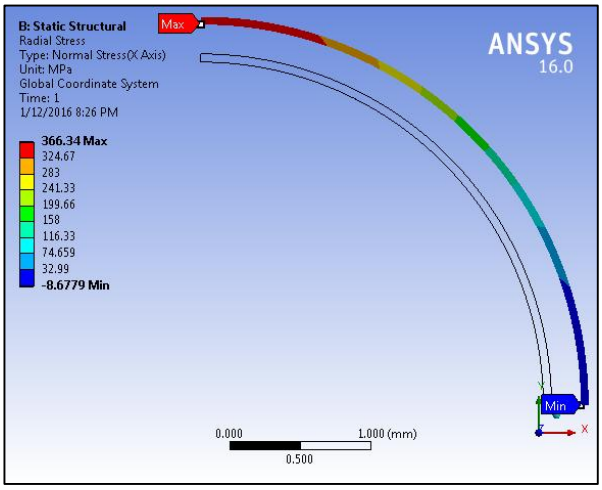

Fig. 5.5. Ansys®16.0 Showing Element Model Radial Stress distribution

International Journal of Engineering Research & Technology (IJERT)
ISSN: 2278-0181
Vol. 5 Issue 01, January-2016

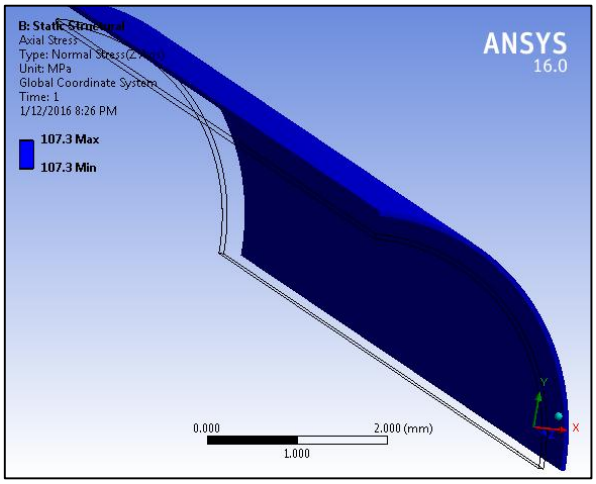

Fig. 5.6. Ansys®16.0 Showing Element Model Axial Stress distribution

Maximum principal stress and maximum value are on the inside surface. Mesh refinement results:

TABLE III. ANSYS® 16.0 MESH REFINEMENT RESULT

		FEA (Element size:0.1mm)	FEA (Element size:0.06mm)	FEA (Element size:0.01mm)
Hoop Stress (M pa)	*Inner Surface*	180.56	180.45	180.45
	Outer Surface	171.73	171.78	171.78
Axial Stress (M pa)	*(Constant)*	107.3	107.3	107.3
Radial Stress (M pa)	*Inner Surface*	-8.6779	-8.6142	-8.6142
	Outer Surface	0.112	0.108	0.108

Our results don't change significantly on refining the mesh. The medium and finest meshes yield virtually identical results. So we'll use the results from the medium mesh (element size of 0.01 mm) to compare with the thick-walled hand calculations.

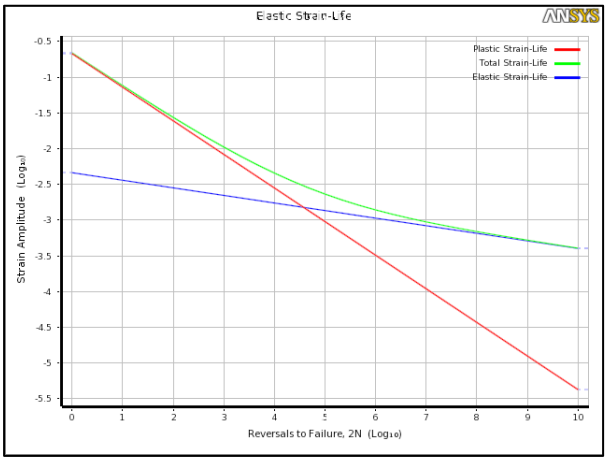

Fig. 5.7. Strain life of the structure steel pressure vessel

Our FEA results compare very well with thick-walled theory where agreement is within 0.01-0.03% with theory. The thin-walled theory is beginning to lose validity. For this geometry, the FEA predictions differ from thin-walled theory by as much as 20%.

The hoop stress varies with the radial position and stress is greater on the inner surface. The hoop stress variation in thick-walled vessels can be depicted as in figure 3.

B. Transient FEA Analysis of Circular Finned Cylindrical Heat Exchanger Pipe.

The following Finned pipe as found in heat exchangers it's a steel pipe with a rolled on finned sheet.

Fig. 5.8.SolidWorks®2015 Modelled circular finned cylindrical heat exchanger pipe

To calculate the transient temperature distribution and stress on a small section or segment of the modeled pipe. Defining the material properties in addition to structural steel.

Assuming, we define a bonded contact between the pipe and circular fin. The two components have a firm connection across the surface array.

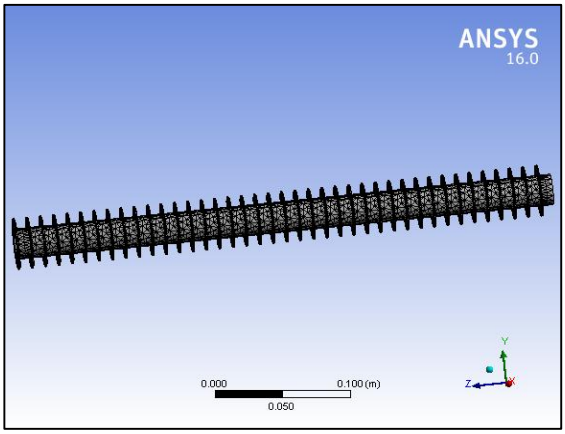

Fig. 5.9.Ansys® 16.0 Showing Meshed model

International Journal of Engineering Research & Technology (IJERT)
ISSN: 2278-0181
Vol. 5 Issue 01, January-2016

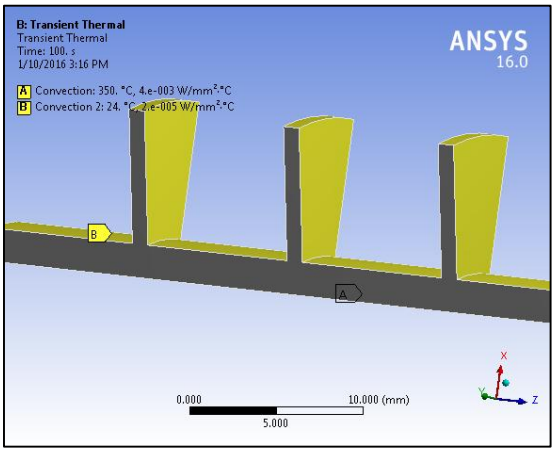

Fig. 5.10.Ansys® 16.0 Showing applied boundary conditions

Defining the mesh thickness between both components as 0.2 millimeters. Finally, defining the thermal boundary conditions, water passes the inner surface at 350^0C and air expels the energy by a forced convection in the outer region, where fins are located.

Convection boundary condition, using a typical value for flowing water in a pipe flow 4000 watts per square meter kelvin. Turning to the outer region, selecting corresponding surfaces and we also select all the attached tangential parts so as to ensure we select all the corresponding surfaces. And we define a convection 20 watts per square meter kelvin with respect to the surrounding air within this region.

Defining the time frame for whole calculation which would be 100 seconds for FEA analysis. On completion, the temperature and the heat flux density dependence on time can be portrayed.

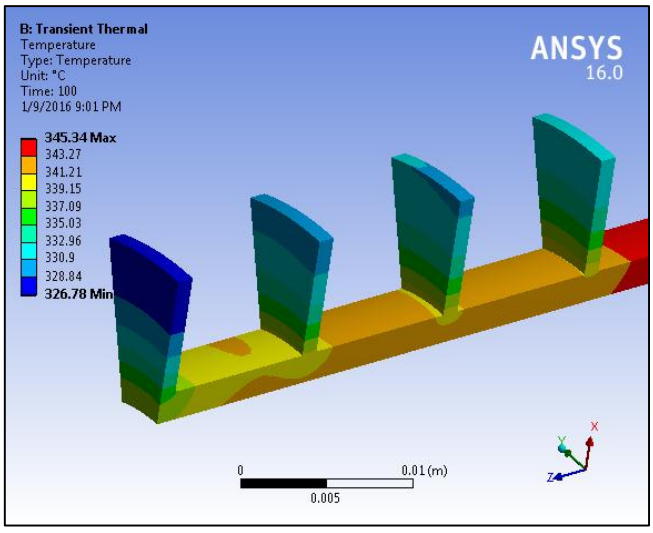

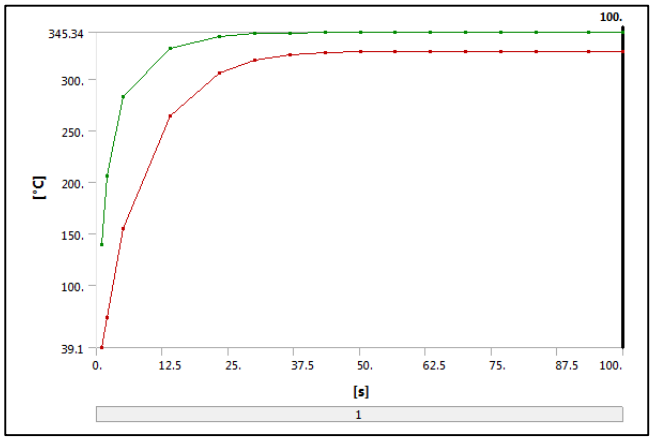

Fig. 5.11.Ansys®16.0 Transient Temperature distribution profile of the circular finned pipe.

In figure 5.11, we can see that about 30 to 40 seconds it settled at its final level with the temperature distribution apparently amounting to between 326^0C and 345^0C.The temperature of about 345^0C on the inside and 326^0C to 335^0C degrees on the outer side of the fins.

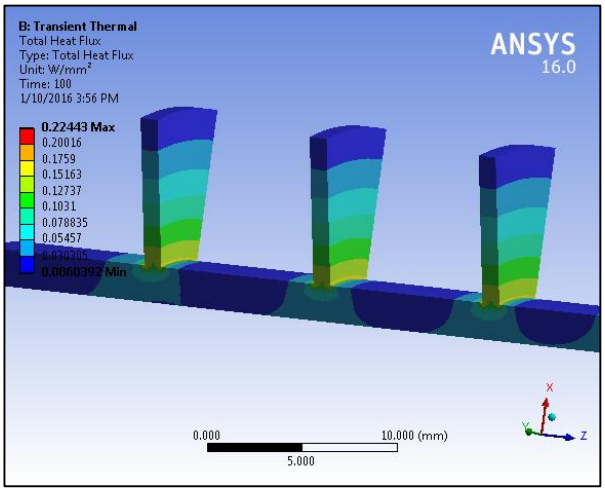

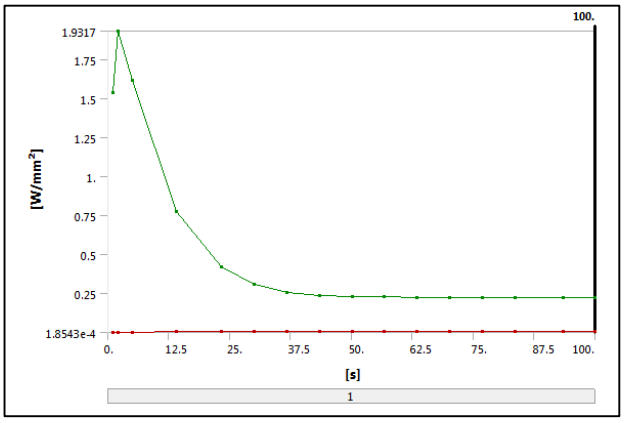

Fig. 5.12.Ansys®16.0 Transient Total Heat flux density of the circular finned pipe.

International Journal of Engineering Research & Technology (IJERT)
ISSN: 2278-0181
Vol. 5 Issue 01, January-2016

The heat flux density we see that as a particularly high heat flux density in the area where the fins begin, i.e., at the transition between the pipe and the fins. The fins have a very large surface area allowing a lot of energy to be discharged.

There is a bottleneck, a high heat flux density at the exact point where the fins begin. Henceforth, it's difficult for the gamma energy to enter the large surface area of the rib.

Improvement of the heat dissipation in this region can be obtained by thickening the root part of the fins, for about an elementary incremental.

For calculation of the thermal expansion and thermal stress based on temperature, temperature distribution and the material mix, coupling static analysis with the transient temperature value analysis.

Now, defining the mechanical boundary conditions by determining where symmetry is found. Mechanical symmetry refers to the absence of deformation and perpendicular to the surface equating to a frictionless support. Assuming that Pipe can move freely in a longitudinal direction. It's only a representative section terms of length. The end should be free so that boundary effects can be taken into account.

Finally, defining the time-dependent boundary conditions with respect to the stress calculation. Taking the default step end time which relates to the final time increment the thermal transient analysis.

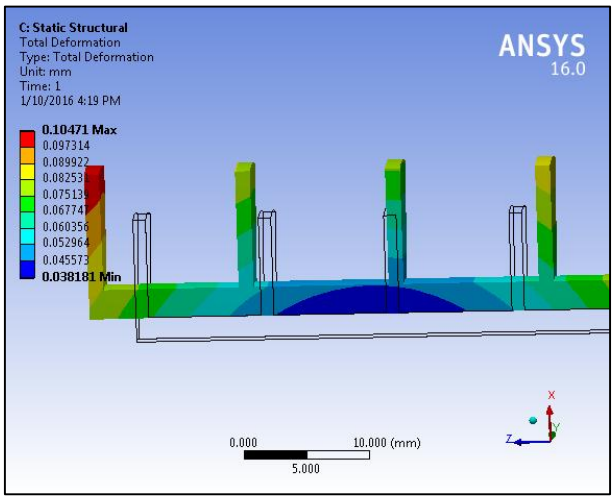

Fig. 5.13. Ansys®16.0 Total deformation of the circular finned pipe

From figure 5.13, we can see a casting boundary effect which displays a radial expansion and an axial movement. At the end, due to the boundary effect, we observe everything tilting in order to produce a slight plate shaped deformation in the outer fin.

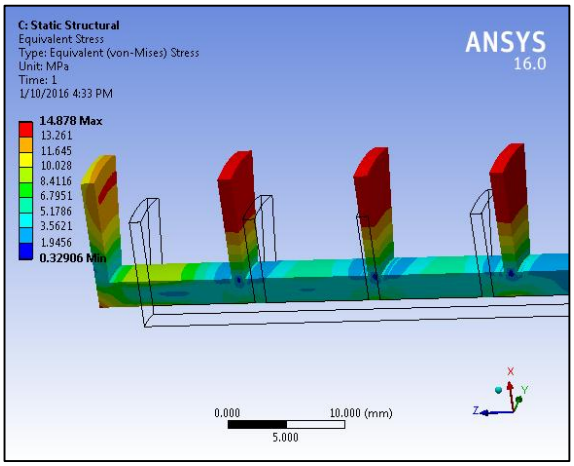

Fig. 5.14.Ansys®16.0 showing the Equivalent Von-Mises Stress on the section of the model.

With respect to stress we're looking at about 15 M Pa in the outer region of the pipe.

VI. RESULT AND DISCUSSIONS

TABLE IV. COMPARISON WITH THICK-WALLED THEORY FROM THE ANALYSIS:

		FEA(Element size:0.01mm)	Analytical Result
Hoop Stress (M pa)	*Inner Surface*	180.45	181.06
	Outer Surface	171.78	172.43
Axial Stress (M pa)	*(Constant)*	107.3	86.21
Radial Stress (M pa)	*Inner Surface*	-8.6142	-8.628
	Outer Surface	0.108	0

The optimal and finest meshes yield identical results. Henceforth, using the results from the optimal mesh (element size of 0.01 mm) to compare with the thick-walled pressure analytical results from table 4.

International Journal of Engineering Research & Technology (IJERT)
ISSN: 2278-0181
Vol. 5 Issue 01, January-2016

TABLE V. DISPLAYING THE TIME DEPENDENCE OF THE TEMPERATURE AND TOTAL HEAT FLUX ANALYSIS RESULTS.

Time [s]	Minimum [°C]	Maximum [°C]	Minimum [W/m²]	Maximum [W/m²]
1	39.1	139.19	185.43	1.54E+06
2	68.3	205.39	700.56	1.93E+06
5	154.49	282.32	2430.5	1.62E+06
14	264.14	329.64	4718	7.78E+05
23.423	305.39	341.16	5586.9	4.20E+05
30.099	317.85	343.85	5850.2	3.08E+05
36.776	323.08	344.8	5960.8	2.59E+05
43.452	325.25	345.14	6006.9	2.39E+05
50.128	326.15	345.26	6026	2.30E+05
56.804	326.52	345.31	6033.8	2.27E+05
63.48	326.67	345.33	6037	2.25E+05
70.156	326.74		6038.3	2.25E+05
76.833	326.76		6038.9	2.25E+05
83.509	326.77		6039.1	2.24E+05
93.509	326.78	345.34	6039.2	2.24E+05
100				2.24E+05

In the above table 5, FEA simulated results of the Temperature (^{0}C) and Heat Flux (W/m^2) is shown in correspondence with the time frame (sec.). Defining the time frame for whole calculation which would be 100 seconds for FEA analysis. On completion, the temperature and the heat flux density start to converge at a point which becomes almost constant over time 63.48 seconds. Thereafter, negligible alteration of values can be observed, while an attempt to simulate in extended time frame.

VII. CONCLUSION

In the thick pressure vessel our FEA results compare very well with thick-walled theory where agreement is within 0.01-0.03% with theory. The thin-walled theory is beginning to lose validity. For this geometry, the FEA predictions differ from thin-walled theory by as much as 20%. The hoop stress varies with the radial position and stress is greater on the inner surface.

In the Circular finned cylindrical heat exchanger pipe, there exists a high heat flux density at the exact point where the fins begin, which results a bottleneck. Henceforth, it's difficult for the gamma energy to enter the large surface area of the rib.

Improvement of the heat dissipation in this region can be obtained by thickening the root part of the fins, for about an elementary incremental size.

ACKNOWLEDGMENT

We have tried our best to present information as clearly as possible using basic terms that I hope will be comprehended by the widest spectrum of researchers, analysts and students for further studies.

Mere acknowledgment may not redeem, we would likewise like to record our gratitude towards our parents and colleague in developing the project, who have willingly helped us out with their abilities.

REFERENCES

[1] Khan, B.H.; *Non-Conventional Energy Resources*,4th ed.; p.p. 1-115; New Delhi; Tata McGraw Hill, 2008.

[2] Neha Tiwari, Appu Kumar Singh, Tejas Vishwakarma, Harshal Sharma & Mohammed Suhail; *Off-feed Axis Solar Concentrating Collector with a β-configuration Stirling Engine*; International Journal of Engineering Research & Technology; vol.3, no.9; sept.(2014).

[3] Garg, H.P. & Prakash, J., *Solar Energy – fundamentals and applications*; 1st revised ed., p.p. 2, p.p. 116-140 & p.p. 418-424; New Delhi; Tata McGraw Hill, 2012.

[4] Singhal, Kothandaraman, C.P., Subramanyan, S.; *Heat and Mass Transfer Data Book*, 8th ed.; p.p.116 & p.p.52-84; New Delhi; New Age International Ltd., 2014.

[5] Sukhatme, S.P. & Nayak, J.K., *Solar Energy - Principles of Thermal Collection & Storage*, 3rd ed.; p.p. 9-69 & p.p. 200-254; New Delhi; Tata McGraw Hill, 2010.

[6] Wade, Paul; *Offset –Fed Parabolic Dish Antennas*, NIBWT, 1998.

[7] Senthikumar, S., Yasodha, N., *Design and Development of a three dimensional compound parabolic concentrator and study of optical and thermal performance*; International Journal of Energy Science; vol.2, no.2, p.p., 64-68, 2012.

[8] Ahmadi, Mohammad Hossien & Hosseinzade, Hadi, *Investigation of Solar Collector Design Parameters Effect onto Solar Stirling Engine Efficiency*, J Applied Mechanic Engineering, vol.1, issue-1, 2012.

[9] Neha Tiwari, Appu Kumar Singh, Tejas Vishwakarma, Harshal Sharma & Mohammed Suhail, *Exhaust Manifold Waste Heat Recovery System of a Single Cylinder Engine*; Applied Mechanics and Materials (Volumes 592 - 594), (10.4028/www.scientific.net/AMM.592-594.1534), Chapter 5: Thermodynamics and Thermal Engineering, Fuel and Diesel, p.p., 1534-1538, 2014.

[10] Gere, J.M., Timoshenko, S.P.; *Mechanics of Materials*, 2nd ed.; p.p.309-312; New Delhi; CBS Publishers & Distributors Pvt. Ltd., 2004.